Contribution No. 6857 from the Arthur Amos Noyes Laboratory, California Institute of Technology, Pasadena, California 91125

Polarized Electronic Spectra of Dirhodium(II) Tetraacetate

VINCENT M. MISKOWSKI,* WILLIAM P. SCHAEFER, BEHZAD SADEGHI, BERNARD D. SANTARSIERO, and HARRY B. GRAY*

Received June 15, 1983

Single-crystal polarized electronic spectra are reported for the Rh^{II} compounds $Rh_2(O_2CCH_3)_4(OH_2)_2$ and $Li_2Rh_2(O_2CCH_3)_4Cl_2 \cdot 8H_2O$. A crystal structure analysis of the latter compound was performed (space group $I4/m$ (No. 87), a = 8.8498 (5) Å, c = 14.5989 (16) Å, Z = 2). The $Rh_2(O_2CCH_3)_4Cl_2^{2-}$ anion resides in a position of C_{4h} site symmetry, and the Rh_2 bond length is 2.397 (1) Å. The two compounds have similar electronic spectra. Absorption bands (ϵ 200–300) attributable to electric-dipole-allowed transitions occur at ~600 and ~650 nm, with x, y, and z polarizations, respectively. The ~600-nm band of the aquo complex is split by ~150 cm^{-1} into x- and y-polarized components, and it shows long progressions in a 300-cm^{-1} excited-state vibration. The corresponding ground-state vibration at 343 cm^{-1} is assigned to the symmetric Rh–O(carboxylate) stretch on the basis of Raman evidence, and the ~600- and ~650-nm absorption systems are assigned to $\pi^*(Rh_2) \rightarrow \sigma^*(Rh\text{–}O)$ and $\delta^*(Rh_2) \rightarrow \sigma^*(Rh\text{–}O)$ transitions. Weak bands (ϵ 10–20) in the 650–800-nm range, structured for both compounds in 300-cm^{-1} progressions, are assigned to spin-forbidden components of $\delta^*, \pi^* \rightarrow \sigma^*(Rh\text{–}O)$. An unstructured x,y-polarized 450-nm (ϵ 200) absorption assigned to $\pi(Rh\text{–}O) \rightarrow \sigma^*(Rh\text{–}O)$ is split by 1200 cm^{-1} in the aquo complex (the splitting is likely due to hydrogen bonding in the lattice). On the basis of solution spectra, the $\sigma(Rh_2) \rightarrow \sigma^*(Rh_2)$ transition is assigned at 220–230 nm (ϵ 17 000) for a variety of $Rh_2(O_2CCH_3)_4X_2$ (X = axial ligand) complexes. With X = Cl^-, Br^-, and I^-, there are additional intense bands (ϵ ~25 000) at 272.5, 291, and 332 nm, respectively, assigned to $\sigma(Rh\text{–}X) \rightarrow \sigma^*(Rh_2)$ transitions. Our conclusions concerning the electronic structural nature of dirhodium(II) tetraacetate complexes are compared in detail with those based on previous experimental and theoretical work.

Introduction

We originally became interested in the electronic and vibrational spectra of $Rh_2(O_2CCH_3)_4$ as a result of the publication of a paper on the polarized single-crystal spectrum of the hydrate by Martin and co-workers.[1] The most interesting of their results was that an x,y-polarized band at ~17 000 cm^{-1}, long assigned[2,3] to a $\pi^*(Rh_2)$ to $\sigma^*(Rh_2)$ transition and now confirmed to have the "right" polarization, exhibited a long vibronic progression in a ~300-cm^{-1} interval. As the ground-state $\nu(Rh_2)$ had been assigned[4] at 320 cm^{-1}, the interpretation seemed to be in good order.

We were not satisfied with this interpretation, however, for two major reasons. First, the assignment of $\nu(Rh_2)$ at 320 cm^{-1} appeared disturbingly high[5] for the Rh–Rh bond length of 2.3855 Å in the hydrate.[6] Second, it seemed most surprising that a formal reduction of the metal–metal bond order from[3,7] 1 to 0.5 in the $\pi^*(Rh_2) \rightarrow \sigma^*(Rh_2)$ excited state should cause such a small reduction in $\nu(Rh_2)$.

We have accumulated arguments and evidence in favor of a reassignment of the 320-cm^{-1} mode to the symmetric Rh–O(carboxylate) stretch. This has the effect of casting doubt on the accepted assignment of the electronic spectrum, as the wrong vibrational mode is Franck–Condon active. Accordingly, we have reinvestigated the polarized electronic spectra of $Rh_2(O_2CCH_3)_4(OH_2)_2$, considerably extending the results of Martin et al.,[1] and we have measured the polarized spectra of a new compound with a lattice favorable for such experiments, $Li_2Rh_2(O_2CCH_3)_4Cl_2 \cdot 8H_2O$ (LRAC). On the basis of these new results, we have concluded that the interpretation of the electronic spectrum of dirhodium(II) tetraacetate requires significant revision.

Experimental Section

Rhodium(II) acetate[8] was converted to extremely large dark green crystals of the dihydrate by slow evaporation of large volumes (0.5–1 L) of a saturated solution of the complex in dilute aqueous acetic acid. Dimensions of the predominant face of the monoclinic crystals $(10\bar{1})$[7] exceeded 2 cm in our largest samples.

Small dark purple plates of the acetonitrile complex were obtained by cooling hot saturated CH_3CN solutions and were stored in small sealed vials in order to retard the loss of CH_3CN. This material was convenient for solution work because of its ready solubility and because it did not introduce H_2O into concentrated CH_3CN solutions.

The compound LRAC, $Li_2Rh_2(O_2CCH_3)_4Cl_2 \cdot 8H_2O$, was prepared by mixing a saturated solution of $Rh_2(O_2CCH_3)_4(OH_2)_2$ in dilute aqueous acetic acid with an equal volume of saturated aqueous LiCl. When the solution was allowed to stand undisturbed for several days, dark grass green crystals grew slowly. The limiting solubility is actually rather low, but crystal growth is slow, and the supersaturated initial solutions can be used for spectroscopic measurements. The only crystal habit observed was a symmetrically axially truncated tetragonal prism, the truncation commonly exaggerated to yield thin axial plates. The plates displayed beautiful uniaxial cross-optic axis figures under a polarizing microscope.

For single-crystal polarized spectra, it was advantageous to select the largest available crystals and polish them with alumina powder down to desired thickness. In this way we obtained $Rh_2(O_2CCH_3)_4(OH_2)_2$ spectra both for $10\bar{1}$ and for a face polished perpendicular to $10\bar{1}$ and including the crystallographic b axis. Because of the large faces on the samples, we had no difficulty establishing base lines in the difficult near-infrared region and could maintain usable noise levels for absorbances as great as 4 in the visible region. All crystals were carefully masked with copper grease.

Both thin and thick axial crystal faces were available from the LRAC crystals as grown. Faces containing the c axis (σ/π faces) were obtained by polishing. Because the crystals were less than a few millimeters in the largest dimension, optical absorption signal/noise levels were considerably lower than for the hydrate.

Low-temperature UV spectra were obtained for $Rh_2(O_2CCH_3)_4(OH_2)_2$ in poly(vinyl alcohol) (PVA) films. Very concentrated PVA/H_2O, formed by stirring solid PVA into hot water, was mixed with saturated hot aqueous $Rh_2(O_2CCH_3)_4(H_2O)_2$, and drops of the mixture were evaporated onto quartz plates. The visible absorption for these thin pale blue-green films is low, but UV absorption is adequate. Spectra of identical films cast without the rhodium com-

(1) Martin, D. S.; Webb, T. R.; Robbins, G. A.; Fanwick, P. E. *Inorg. Chem.* **1979**, *18*, 475.
(2) Dubicki, L.; Martin, R. L. *Inorg. Chem.* **1970**, *9*, 673.
(3) (a) Norman, J. G.; Kolari, H. J. *J. Am. Chem. Soc.* **1978**, *100*, 971. (b) Norman, J. G.; Renzoni, G. E.; Case, D. A. *Ibid.* **1979**, *101*, 5256.
(4) Ketteringham, A. P.; Oldham, C. *J. Chem. Soc., Dalton Trans.* **1973**, 1067.
(5) Trogler, W. C.; Gray, H. B. *Acc. Chem. Res.* **1978**, *11*, 232.
(6) Cotton, F. A.; DeBoer, B. G.; LaPrade, M. D.; Pipal, J. R.; Ucko, D. A. *Acta Crystallogr., Sect. B* **1971**, *B27*, 1664.
(7) (a) Cotton, F. A.; Felthouse, T. R. *Inorg. Chem.* **1981**, *20*, 584, 600. (b) Felthouse, T. R. *Prog. Inorg. Chem.* **1982**, *29*, 73.
(8) Rempel, G. A.; Legzdins, P.; Smith, H.; Wilkinson, G. *Inorg. Synth.* **1972**, *13*, 90.

0020-1669/84/1323-1154$01.50/0

Table I. Crystal Data

$Li_2Rh_2(O_2CCH_3)_4Cl_2 \cdot 8H_2O$	fw = 670.90
space group $I4/m$ (No. 87)	$Z = 2$
$a = 8.8498$ (5) Å	$t = 21$ °C
$c = 14.5989$ (16) Å	ρ(measd) = 1.90 (3) g/cm^3
$V = 1143.4$ (3) Å^3	ρ(calcd) = 1.91 g/cm^3
λ(Mo Kα) = 0.710 69 Å	$\mu = 16.7$ cm^{-1}

Table II. Final Atomic Parameters[a]

atom	x	y	z	B_{eq}, Å^2
Li	1/2	0	1/4	3.45 (6)[b]
Rh	0	0	821.2 (1)	1.89 (1)[b]
Cl	0	0	2602.8 (5)	2.58 (1)[b]
C(1)	1470 (2)	2524 (2)	0	2.47 (3)[b]
C(2)	2287 (4)	3983 (3)	0	3.63 (5)[b]
O	1153 (1)	1957 (1)	771 (1)	2.69 (2)[b]
W[c]	3854 (2)	1587 (2)	1932 (1)	4.06 (2)[b]
H(1)	1608 (57)	4676 (61)	0	10.2 (17)
H(2)	2763 (38)	4180 (32)	535 (19)	7.8 (8)
HW(1)	3065 (32)	1585 (32)	1692 (17)	5.9 (8)
HW(2)	4084 (38)	2280 (39)	1990 (22)	8.2 (12)

[a] Coordinates have been multiplied by 10^4. [b] $B_{eq} = (8\pi^2/3)\Sigma_i\Sigma_j(U_{ij}(a_i^*a_j^*)\vec{a}_i\vec{a}_j)$; $\sigma(B_{eq}) = (B_{eq}/3(6^{1/2}))\Sigma_i(\sigma(U_{ii})/U_{ii})$. [c] Oxygen atom of lattice H_2O.

pound (a weak featureless rising background) were subtracted from the raw data. The background is noticeably temperature dependent.

Infrared and far-infrared spectra were obtained on a Perkin-Elmer 180 instrument. Samples were petroleum jelly mulls held between KBr or polyethylene plates. Raman spectra were recorded with a Spex 14018 double monochromator with photon-counting electronics with excitation by an argon ion laser or an argon ion excited dye laser, and with a 90° scattering geometry.

X-ray Structural Determination

Preliminary photographs of single crystals of LRAC indicated a centered lattice and tetragonal unit cell; the systematic absences $h + k + l = 2n + 1$ and the Laue symmetry $4/m$ are consistent with space groups $I4$, $I\bar{4}$, and $I4/m$. The centrosymmetric space group $I4/m$ (No. 87) was chosen and confirmed by the successful structure solution and refinement.

A crystal 0.29 × 0.20 × 0.17 mm was carefully centered on a locally modified Syntex $P2_1$ diffractometer with a graphite monochromator (Mo Kα radiation). Cell dimensions were obtained from the least-squares fit, constrained to tetragonal symmetry, of 2θ values for 15 reflections ($31° < 2\theta < 51°$); the 15 reflections were each centered at $\pm 2\theta$ and the $|2\theta|$ values averaged. Crystal data are given in Table I.

Data were collected in the range $3° < 2\theta < 65°$ by a θ–2θ scan at 2°/min from 1° below the Kα_1 peak to 1° above the Kα_2 peak. Background was counted for half the scan time at each end of the scan. Three reflections were monitored every 97 reflections; they showed no significant changes in intensity. The 2559 reflections were corrected for Lorentz and polarization factors, but not for absorption, and merged to give 1108 independent reflections, of which 1098 had $F_o^2 > 0$ and 1029 had $F_o^2 > 3\sigma(F_o^2)$.

The structure was solved by Patterson and Fourier methods and refined by least squares using programs of the CRYM system. The final R index ($\sum||F_o| - |F_c||/\sum F_o$) was 0.024 for all positive reflections and 0.023 for those reflections with $F_o^2 > 3\sigma(F_o)^2$. The goodness of fit ($[\sum w(F_o^2 - F_c^2)^2/(n-p)]^{1/2}$; n = number of data, p = number of parameters) is 2.13 for $n = 1108$ and $p = 55$; a parameter for the correction of isotropic secondary extinction was refined, final value $g = 1.30\ (5) \times 10^{-6}$. Final values for the atomic parameters are given in Table II. Selected bond lengths and angles are in Table III.

LRAC Structure

The LRAC structure is similar to that of many other carboxylate-bridged binuclear rhodium complexes.[7,9] Both the Rh–Rh and Rh–Cl distances agree well with those observed in an unpublished study of the same anion as the guanadinium salt.[9b] The Rh–Rh distance, 2.397 (1) Å, is very similar to that of the aquo adduct, 2.3855 (5) Å.[6]

Table III. Important Distances and Angles

atom	atom	dist, Å	atom	atom	atom	angle, deg
Rh	Rh	2.397 (1)	Cl	Rh	O	92.06 (3)
Rh	Cl	2.601 (1)	Rh	Rh	O	87.94 (3)
Rh	O	2.034 (1)	O	C(1)	O	125.3 (2)
O	C(1)	1.267 (2)	O	C(1)	C(2)	117.3 (2)
C(1)	C(2)	1.496 (4)	Rh	O	C(1)	119.4 (1)

It is noteworthy that Ru($II^1/_2$) carboxylates show[10] metal–axial ligand bond lengths that are virtually identical with those of the Rh^{II} carboxylates, both for Cl^- and OH_2. The extremely long metal–chloride bonds presumably reflect the trans influence of the strong metal–metal bonding. But the effect is not modulated by large changes in metal–metal distance; the Ru($II^1/_2$) metal–metal bond lengths are over one-tenth of an angstrom shorter than those of the Rh^{II} compounds. Theoretical calculations[3b] indicate that metal–chloride π interactions are negligible in these compounds, which is consistent with the structural observations. Apparently, the trans effect is purely σ, because the axial-ligand bonding is not sensitive to metal–metal π and δ interactions that are responsible[3] for the variation in metal–metal distance.

Vibrational Spectra

We are aware of three assignments of rhodium–rhodium stretching frequencies for rhodium(II) carboxylates. Kharitonov et al.[11a] placed $\nu(Rh_2)$ at 155 cm^{-1} for $Rh_2(O_2CCH_3)_4(H_2O)_2$ and calculated $k(Rh_2) = 0.67$ mdyn/Å. San Filippo and Sniadoch[12] tentatively suggested $\nu(Rh_2) = 170$ cm^{-1} for $Rh_2(O_2CCH_3)_4(CH_3OH)_2$. Finally, Ketteringham and Oldham (KO)[4] assigned $\nu(Rh_2)$ in the region 288–351 cm^{-1} for a variety of rhodium carboxylates, with $\nu(Rh_2) = 320$ cm^{-1} for $Rh_2(O_2CCH_3)_4(H_2O)_2$. It is unfortunate that the KO Rh_2 frequency was adopted by Nakamoto[13] in the third edition of his text, because the evidence now available shows clearly that it is far too high.

A $\nu(Ru_2)$ of 325.7 cm^{-1} is firmly established[14] for $Ru_2(O_2CCH_3)_4(OH_2)_2^+$; since this ion has[15] a metal–metal bond 0.137 Å shorter than that of[6] $Rh_2(O_2CCH_3)_4(OH_2)_2$, a much lower $\nu(M_2)$ would be expected for the latter. Furthermore, Garner and co-workers[16] have assigned $\nu(Rh_2) = 184$ cm^{-1} for $Rh_2(mhp)_4$ (H(mhp) = 6-methyl-2-hydroxypyridine), where the assignment is aided by the availability of a large series of isostructural compounds with different metals. As this compound has[16] a Rh–Rh bond 0.026 Å shorter than that of $Rh_2(O_2CCH_3)_4(OH_2)_2$, the incompatibility of the KO assignment[4] is again apparent.

The $\nu(Rh_2)$ assignments in the 150–170-cm^{-1} range[11,12] are obviously to be preferred, thereby leaving us with the question of how to interpret the features observed by KO.[4] This proves to be an important point in our interpretation of the electronic spectra (vide infra).

(9) (a) Koh, Y. B.; Christoph, G. G. *Inorg. Chem.* **1979**, *18*, 1122. (b) Spies, G. H.; Christoph, G. G., private communication.

(10) (a) Bino, A.; Cotton, F. A.; Felthouse, T. R. *Inorg. Chem.* **1979**, *18*, 2599. (b) Marsh, R. E.; Schomaker, V. *Ibid.* **1981**, *20*, 299.

(11) (a) Kharitonov, Y. Y.; Mazo, G. Y.; Knyazeva, N. A. *Russ. J. Inorg. Chem. (Engl. Transl.)* **1970**, *15*, 739. (b) Mazo, G. Y.; Baranovskii, I. B.; Shchelokov, R. N. *Ibid.* **1979**, *24*, 1855. Work reported in ref 11b also establishes the infrared-active ν(Rh–Cl) of $Rh_2(O_2CR)_4Cl_2^{2-}$ at 170–180 cm^{-1}.

(12) San Filippo, J., Jr.; Sniadoch, H. J. *Inorg. Chem.* **1973**, *12*, 2326.

(13) Nakamoto, K. "Infrared and Raman Spectra of Inorganic and Coordination Compounds", 3rd ed.; Wiley: New York, 1978; p 329.

(14) Clark, R. J. H.; Ferris, L. T. H. *Inorg. Chem.* **1981**, *20*, 2759.

(15) Bino, A.; Cotton, F. A.; Felthouse, T. R. *Inorg. Chem.* **1979**, *18*, 2599.

(16) Clegg, W.; Garner, C. D.; Al-Samman, M. H. *Inorg. Chem.* **1982**, *21*, 1897 and references therein.

Table IV. Solution Raman Data for $M_2(O_2CCH_3)_4$ Complexes

compd (concn, M)	$\Delta\tilde{\nu}$,[a] cm^{-1}	rel intens	ρ	assgnt
$Cu_2(O_2CCH_3)_4$	945	0.34	0.10 ± 0.02	$\nu_{a_{1g}}$(C-C)
(1×10^{-2} in CH_3CN)	312	1.0	0.10 ± 0.02	$\nu_{a_{1g}}$(Cu-O)
$Rh_2(O_2CCH_3)_4$	951	0.12	0.14 ± 0.02	$\nu_{a_{1g}}$(C-C)
(2×10^{-2} in CH_3CN)	345	1.0	0.12 ± 0.02	$\nu_{a_{1g}}$(Rh-O)
	323	0.33	0.8 ± 0.1	ν_{dp}(Rh-O)
$Rh_2(O_2CCH_3)_4$	953	0.5	~0.1	$\nu_{a_{1g}}$(C-C)
(4×10^{-3} in H_2O)	343	1.0	~0.1	$\nu_{a_{1g}}$(Rh-O)

[a] Excitation λ 514.5 nm.

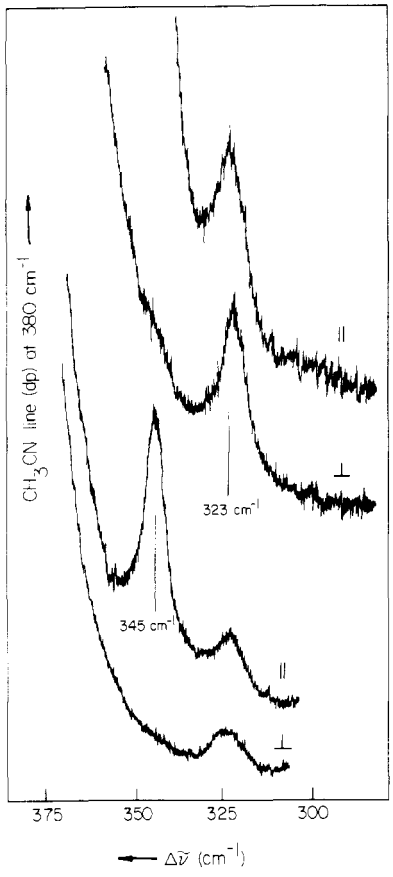

Figure 1. Raman (488-nm excitation) polarization data for ν(Rh–O) modes of $Rh_2(O_2CCH_3)_4$ in CH_3CN solution (spectral slit width 5 cm^{-1}). The two upper spectra were recorded with longer accumulation times.

We attacked this problem by measuring solution Raman spectra, which are useful because they yield depolarization ratios. The rhodium complexes are rather poor scatterers and require high concentrations. We see no resonance effects with visible absorption bands; neither scattering intensities nor depolarization ratios show strong dispersion in the 450–600-nm range. (Because of the weakness of the scattering and large self-absorption corrections, we cannot exclude weak resonance or antiresonance intensity contributions.) The conclusion that these are essentially "nonresonance" spectra follows more simply from the fact that both solutions and solids[12] yield Raman spectra showing very many lines; there is no special enhancement of a few modes.

Crucial data are summarized in Table IV and illustrated in Figure 1. Our best data were obtained in CH_3CN, a better solvent for $Rh_2(O_2CCH_3)_4$ than H_2O. This solvent has the added advantages that $Cu_2(O_2CCH_3)_4$ solutions have an electronic spectrum characteristic of dimers,[17] allowing a direct

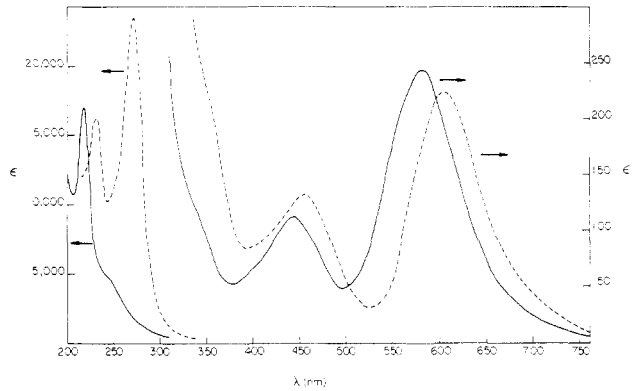

Figure 2. Solution electronic spectra for $Rh_2(O_2CCH_3)_4$ in aqueous solution (—) and $Rh_2(O_2CCH_3)_4Cl_2^{2-}$ in 50% saturated LiCl(aq) (--).

comparison, and that CH_3CN tends to bind in a near-linear fashion[18] so that D_{4h} symmetry should be a good approximation for the $M_2(O_2CCH_3)_4(NCCH_3)_2$ complexes.

The major line observed in the 300–350-cm^{-1} region probably corresponds to the "very intense" feature reported by KO.[4] It is strongly polarized, $\rho \simeq 0.1$. Now, for our analyzing geometry, the theoretical[19] value of ρ for the Rh–Rh stretch (single-axis polarized) is $^1/_3$, whereas a completely x,y-polarized ($\alpha_{zz} = 0$) totally symmetric mode should have $\rho = {}^1/_8$. For comparison, we also determined ρ for the acetate C–C stretch near[20] 950 cm^{-1} (Table IV), which is a good example of a mode that is expected to be purely x,y-polarized. Clearly, both lines accord with theory for totally symmetric x,y-polarized features.

For M–M–O angles of 90°, kinematic (G matrix) mixing between M–M and M–O modes becomes very small[21] in the "copper acetate" structure. (It would be rigorously zero for M_2O_8 with 90° angles.) Thus, the symmetric metal–oxygen stretch should be a purely equatorial (x,y) mode for $Rh_2(O_2CCH_3)_4(OH_2)_2$ in the absence of resonance effects. Clearly, this is the mode we are observing. The frequency is reasonable. The symmetric ν(M–O) modes are established at 371 cm^{-1} for[14] $Ru_2(O_2CCH_3)_4(OH_2)_2^+$, at 321 cm^{-1} for[22] $Mo_2(O_2CCH_3)_4$, and at[23] 323 cm^{-1} for $Cu_2(O_2CCH_3)_4(OH_2)_2$. Moreover, copper isotope substitution results indicated[23] ν(Cu–O) vibrational modes in the 300–400-cm^{-1} range for a variety of copper carboxylates.

Far-infrared spectra show two lines each in the 300–400-cm^{-1} region for $Cu_2(O_2CCH_3)_4(OH_2)_2$ (373 and 327 cm^{-1}) and $Rh_2(O_2CCH_3)_4(OH_2)_2$ (~380 and 342 cm^{-1}). Together with other workers,[11,20,21,23,24] we assign these as the infrared-active (e_u, a_{2u}) ν(M–O(carboxylate)) modes. The higher frequency mode of the Rh^{II} compound is split into two components (386 and 374 cm^{-1}), suggesting that it is e_u (split by the crystal field). This ordering of ν(M–O) modes turns out to be in agreement with the calculations of Cotton et al.[21] for Mo_2O_8 (modeling $Mo_2(O_2CCH_3)_4$). We particularly note that the close agreement between assigned a_{1g} and a_{2u} frequencies is reasonable, because both correlate to the a_{1g} "monomer" (RhO_4) mode.

(17) Dubicki, L.; Martin, R. L. *Inorg. Chem.* **1966**, *5*, 2203.
(18) Riley, P. E.; Capshew, C. E.; Pettit, R.; Davis, R. E. *Inorg. Chem.* **1978**, *17*, 408.
(19) Behringer, J. In "Raman Spectroscopy Theory and Practice"; Szymanski, H. A., Ed.; Plenum Press: New York, 1967; p 168.
(20) Heyns, A. M. *J. Mol. Struct.* **1972**, *11*, 93.
(21) Bratton, W. K.; Cotton, F. A.; DeBean, M.; Walton, R. A. *J. Coord. Chem.* **1971**, *1*, 121.
(22) Hutchinson, B.; Morgan, J.; Cooper, C. B., III; Mathey, Y.; Shriver, D. F. *Inorg. Chem.* **1979**, *18*, 2048.
(23) (a) Lever, A. B. P.; Ramaswamy, B. S. *Can. J. Chem.* **1973**, *51*, 514. (b) Mathey, Y.; Greig, D. R.; Shriver, D. F. *Inorg. Chem.* **1982**, *21*, 3409.
(24) Moszner, M.; Ziolkowski, J. J. *Bull. Acad. Pol. Sci., Ser. Sci. Chim.* **1976**, *23*, 433.

Table V. Solution Electronic Spectra of $Rh_2(O_2CCH_3)_4$[a]

solvent	$\pi^*(Rh_2) \rightarrow \sigma^*(Rh\text{-}O)$	$\pi(Rh\text{-}O) \rightarrow \sigma^*(Rh\text{-}O)$	not assgnd	$\sigma(Rh\text{-}X) \rightarrow \sigma^*(Rh_2)$	$\sigma(Rh_2) \rightarrow \sigma^*(Rh_2)$
CH_3CN	552 (235)	437 (112)	390 (60 sh), 340 (130 sh), 250 (6000 sh)		221 (18 400)
H_2O	585 (240)	443 (112)	400 (60 sh), 340 (120 sh), 250 (4000 sh)		218.5 (17 000)
50% satd[b] LiCl(aq)	606 (220)	455 (130)	410 (100 sh), 355 (200 sh)	272.5 (23 500)	233 (16 000)
50% satd[b] LiBr(aq)	612 (220)	455 (140)	360 (300 sh)	291 (27 500)	
50% satd[b,c] NaI(aq)	621 (315)	460 (360 sh)		332 (27 000)	

[a] Entries are λ_{max} in nm with ϵ values in parentheses. [b] Very high halide concentrations were necessary to ensure complete formation of the bis(halide) complexes. Solvent absorption resulted in absorption cutoffs at 220, 250, and 290 nm for the chloride, bromide, and iodide complexes, respectively. [c] Measured under N_2 atmosphere.

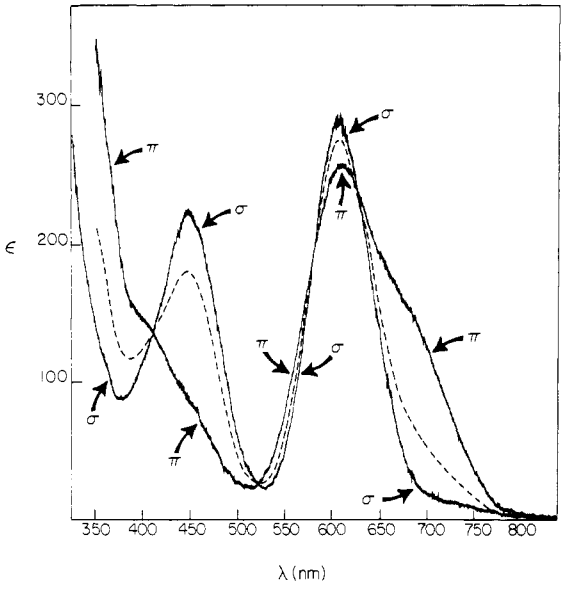

Figure 3. Room-temperature polarized electronic spectra for a 17 μm thick crystal of $Li_2Rh_2(O_2CCH_3)_4Cl_2 \cdot 8H_2O$. Dashed line indicates $\epsilon(\text{isotropic}) = {}^1/_3(\epsilon(\pi) + 2\epsilon(\sigma))$.

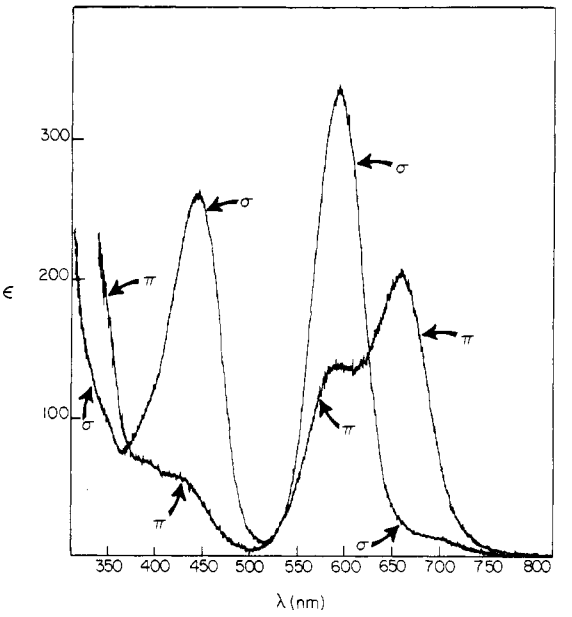

Figure 4. Polarized electronic spectra of LRAC at 20 K (17-μm crystal).

We can add finally that the depolarized line observed at $\Delta\tilde{\nu} = 323$ cm^{-1} for CH_3CN solutions of $Rh_2(O_2CCH_3)_4$ is indicated to be the b_{1g} ν(Rh–O) mode, according to Cotton's[21] calculations, but we have no experimental basis for excluding assignment to the e_g ν(Rh–O) mode. The apparent absence[25] of a depolarized line for our other samples (Table IV) may simply be due to the low intensity of Raman scattering for these solutions; our sensitivity for detection of weak lines was low. The published[26] Raman spectrum of a nucleotide complex of rhodium acetate in aqueous solution has lines at 337 and 319 cm^{-1}, which probably correspond to Rh–O stretches.

Solution Electronic Spectra

Solution electronic absorption spectra of rhodium acetate and related compounds have been reported by many authors.[2,27,28] In Figure 2 spectra are shown that will facilitate later discussions; and the data are summarized in Table V. Some of the UV spectral results are new, and all of our visible absorption measurements are in reasonable agreement with previous determinations. Figure 2 shows two poorly defined shoulders (~350 and ~400 nm; also see Table V) that have not been mentioned previously in the literature.

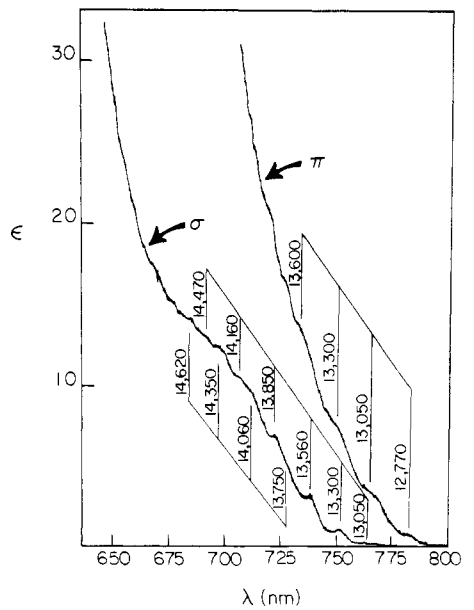

Figure 5. Polarized electronic spectra of LRAC at 20 K (170-μm crystal).

(25) The Raman spectrum of $Rh_2(O_2CCH_3)_4$ in CH_3CN also shows a weak depolarized component of ν(C–C) at $\Delta\tilde{\nu} = 947$ cm^{-1}. A poorly defined shoulder at $\Delta\tilde{\nu} \sim 160$ cm^{-1} is probably $\nu(Rh_2)$. Unfortunately, the sharply rising background prevented us from determining the depolarization ratio.

(26) Moller, M. R.; Bruck, M. A.; O'Connor, T.; Armatus, F. J., Jr.; Knolinski, E. A.; Kottmair, N.; Tobias, R. S. *J. Am. Chem. Soc.* **1980**, *102*, 4589.
(27) (a) Johnson, C. A.; Hunt, H. R.; Neumann, H. M. *Inorg. Chem.* **1963**, *2*, 960. (b) Wilson, C. R.; Taube, H. *Ibid.* **1975**, *14*, 405.
(28) (a) Drago, R. S.; Tanner, S. P.; Richman, R. M.; Long, J. R. *J. Am. Chem. Soc.* **1979**, *101*, 2897. (b) Drago, R. S.; Long, J. R.; Cosmano, R. *Inorg. Chem.* **1982**, *21*, 2196.

Single-Crystal Spectra

First, we shall present our observations on the single-crystal electronic spectra of LRAC and $Rh_2(O_2CCH_3)_4(OH_2)_2$. Interpretation will follow, considering all of the data at once, as each compound provides some information not available for the other.

LRAC. Visible single-crystal spectra of LRAC at room and low temperatures are shown in Figures 3 and 4, and Figure 5 shows the polarized near-infrared spectra obtained for a thick crystal at low temperature. The axial spectrum, for both thick and thin crystals, is identical with the σ spectrum, indicating electric dipole selection rules to be valid. The tetragonal lattice of LRAC then provides a simple separation of the electric dipole transitions into those allowed parallel to molecular z (the Rh–Rh axis), appearing in the π spectrum, and those allowed perpendicular to z, appearing in the σ (and axial) spectra. The site symmetry is C_{4h}; the only difference in electric dipole selection rules from D_{4h} is that transitions transforming as A_{1u} in D_{4h} correlate to A_u in C_{4h} and therefore become allowed in molecular z (π) polarization.

The room-temperature data (Figure 3) can be compared to the room-temperature solution spectrum of $Rh_2(O_2CCH_3)_4Cl_2^{2-}$ (Figure 2) via ϵ(isotropic) = $^1/_3(\epsilon(\pi) + 2\epsilon(\sigma))$. The calculated isotropic spectrum is also shown in Figure 3. Clearly, the solution and crystal chromophores are very similar.

There are three dominant visible absorption bands. At low temperature, these fall at 659 nm (π (z) polarized), 593 nm (σ (x, y) polarized), and 448 nm (σ (x, y) polarized). All three systems have temperature-independent integrated intensities in their allowed polarizations. Note, however, that the 593-nm system has an extremely temperature-dependent π (z) polarized component, which therefore must represent vibronically induced intensity. The 448-nm system also has some rather weak π-polarized intensity. Slightly to higher energy are two predominantly π- (z-) polarized systems (~400 and ~350 nm). The 400-nm band definitely seems to decrease in intensity at low temperature; the 350-nm system may also, but it is difficult to tell in the latter case because of the behavior of the predominantly π- (z-) polarized background, which blue shifts as the temperature decreases.

Figure 5 shows that a very weak low-energy absorption system is vibronically structured. The σ system is better resolved. It appears to maximize near 710 nm and has its 0–0 at 13 050 cm^{-1}. Spectra of crystals that were three times thicker did not show any additional absorption to lower energy. All of the structures can be catalogued in terms of long progressions in a ~300-cm^{-1} frequency, but two origins are necessary. Because of the large Franck–Condon factors, our assignment of the origin of the second progression, which is ~700 cm^{-1} to higher energy of the first origin, must be regarded as highly tentative.

Structure also is observed in π polarization, indicating a lower energy origin (12 770 cm^{-1}). Predominant structure is again in a ~300-cm^{-1} mode, but details are obscured by the tail of the much more intense unstructured π-polarized band to higher energy.

$Rh_2(O_2CCH_3)_4(OH_2)_2$. Polarized single-crystal spectra of the aquo complex are shown in Figures 6 and 7. Our data in π and σ_1 polarizations are in agreement with those given by Martin et al.[1] but extend farther into the near-infrared region and have a somewhat better signal/noise ratio, allowing us to detect some structure in π polarization not seen previously. Our data in σ_2 polarization (orthogonal to π and σ_1) are new (this is the polarization introduced by Rice, Wilson, and Solomon (RWS)[29] for the isomorphous $Cr_2(O_2CCH_3)_4(OH_2)_2$). With the additional experimental information, we have followed RWS in attempting to relate the polarization data to molecular x, y, and z axes. Our analysis indicates that the "best" axes, in terms of avoiding artifacts such as negative absorbances, place z parallel to the metal–metal axis and x and y parallel to O–Rh–O directions. The transformation matrix

$$\begin{pmatrix} \pi \\ \sigma_1 \\ \sigma_2 \end{pmatrix} = \begin{pmatrix} 0.709 & 0.001 & 0.289 \\ 0.001 & 0.999 & 0 \\ 0.290 & 0 & 0.710 \end{pmatrix} \begin{pmatrix} x \\ y \\ z \end{pmatrix}$$

is identical with the one RWS reported,[29] as a result of the close structural similarity.[6] Transformed low-temperature spectra are shown in Figure 8.

The structural basis for these axes is that the M–O(carboxylate) bonds divide into 2 planes with "short" (our x) and "long" (our y) bonds. The distinction is evident in the $Rh_2(O_2CCH_3)_4(OH_2)_2$ structure[6] but somewhat better defined in more recent structures of the isomorphous Cr^{II} [30] and Cu^{II} [31]

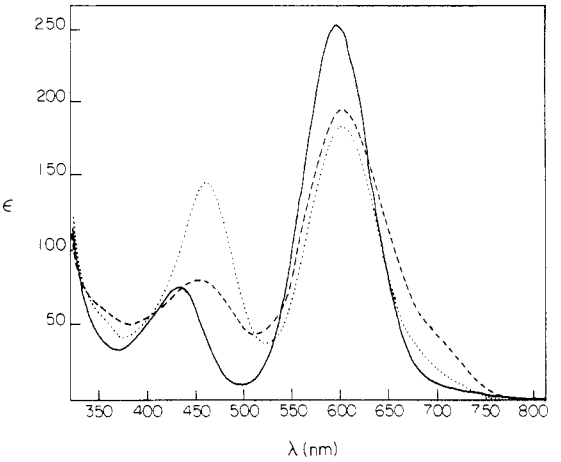

Figure 6. Room-temperature polarized electronic spectra for $Rh_2(O_2CCH_3)_4(OH_2)_2$ single crystals. Polarizations: σ_1 (—); π (···); σ_2 (--). The σ_1 data were obtained from a crystal that was 9.4 μm thick, whereas the crystal for σ_2 data was 15.6 μm thick.

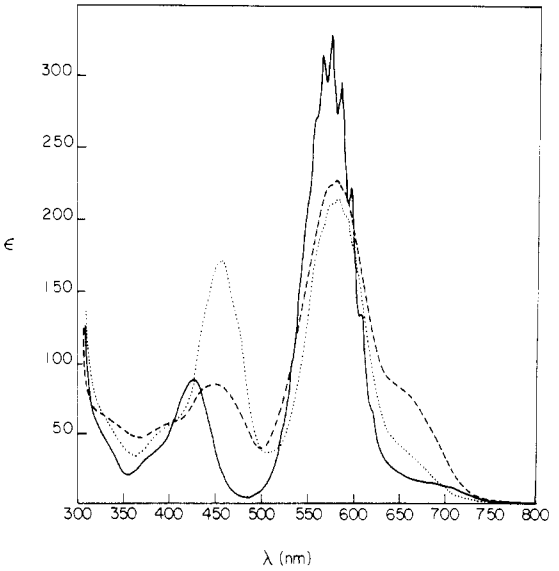

Figure 7. Polarized electronic spectra for $Rh_2(O_2CCH_3)_4(OH_2)_2$ single crystals at 15 K (notation and crystal thicknesses as in Figure 6).

(29) Rice, S. F.; Wilson, R. B.; Solomon, E. I. *Inorg. Chem.* **1980**, *19*, 3425.

(30) Bernard, M.; Coppens, P.; DeLucia, M. L.; Stevens, E. D. *Inorg. Chem.* **1980**, *19*, 1924.

(31) Brown, G. M.; Chidabaram, R. *Acta Crystallogr., Sect. B* **1973**, *B29*, 2393.

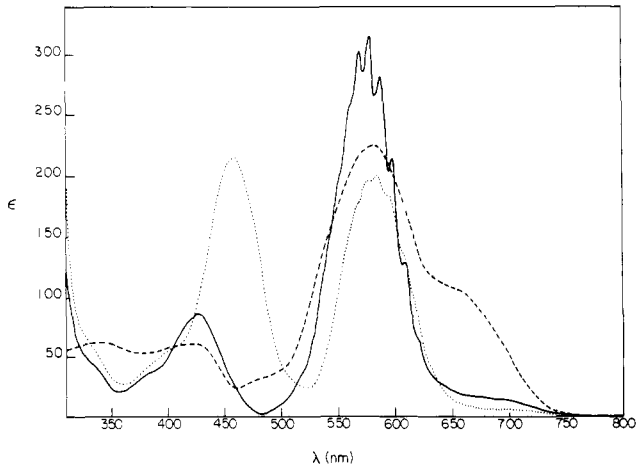

Figure 8. Data of Figure 7 after resolution to molecular axis (see text) polarizations: x (···); y (—); z (- -).

compounds. Thus, the long bonds for $Cr_2(O_2CCH_3)_4(OH_2)_2$ are[30] 2.0327 (7) and 2.0301 (8) Å, while the short bonds are 2.0162 (7) and 2.0039 (7) Å. The reason for this distinction is that the carboxylate oxygens involved in the long metal–oxygen bonds (but not those involved in short ones) form hydrogen bonds[6,30,31] to water ligands of adjacent dimer molecules. Although the hydrogen bonds were not directly detected in the rhodium structure,[6] the close isomorphism of all these structures suggests that they are present. We note that the $Rh_2(O_2CH)_4(OH_2)_2$ calculation by Norman et al.[3a] could not have predicted these axes because it averaged the Rh–O(carboxylate) bond lengths and did not, of course, include the hydrogen bonds.

The resolved data (Figure 8) are of special interest, particularly as they show that the ~660-nm band is nicely segregated into z polarization. Note, however, that a minimum appears in the resolved z spectrum near the resolved x maximum at ~450 nm; this is most likely an artifact, and it may be removed by a rotation of molecular x, z axes by ~20° in the plane perpendicular to y. It must be emphasized that in the $\bar{1}$ (C_i) site symmetry of $Rh_2(O_2CCH_3)_4(OH_2)_2$ all transitions need not be polarized along a single orthogonal set of axes. We simply assert that our choice of such axes makes chemical sense and does not lead to any gross contradictions.

The crystal absorption spectra of the hydrate are qualitatively but not quantitatively similar to those of LRAC. One key difference is that the integrated absorption intensity does not decrease notably in any polarization as the temperature decreases; all absorptions appear to be electric dipole allowed, presumably because of the low site symmetry.

This is most notable for the ~580-nm system. The y component shows a nicely defined progression in a frequency interval of ~300 cm^{-1}, as reported by Martin.[1] The x component shows very similar but somewhat more poorly defined structure; the maxima coincide with minima in the y spectra, so the x and y components are assigned to an x,y-polarized transition split by 150 cm^{-1}.

The z component is considerably broader and unstructured; essentially all of the structure in the π and σ_2 spectra (Figure 7) is carried into the x spectrum in the molecular axis resolution (Figure 8). Comparison to the LRAC spectra (Figures 3 and 4) suggests to us that the z-polarized intensity represents intensity stealing (from higher energy z-polarized transitions) that has become allowed by a static distortion (rather than a vibronic mechanism) in the low site symmetry; the lack of structure may reflect superposition of contributions from both x and y components.

A z-polarized transition is again observed ~2000 cm^{-1} to lower energy of the x,y-polarized system. A trace of structure, again in a roughly 300-cm^{-1} interval, is observed between 650 and 700 nm.

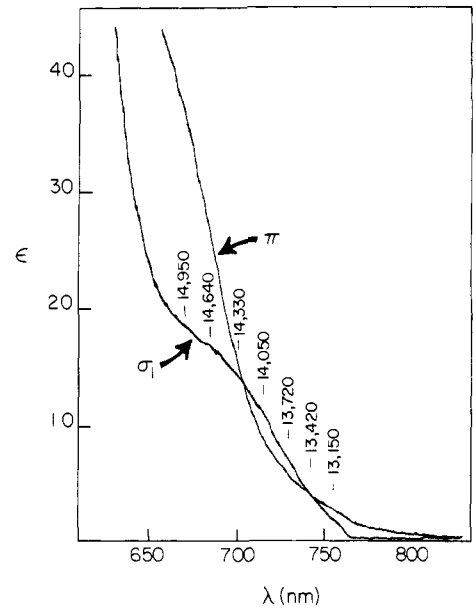

Figure 9. Polarized electronic spectra of a 40 μm thick single crystal of $Rh_2(O_2CCH_3)_4(OH_2)_2$ at 15 K.

A well-defined weakly y-polarized system is observed at still lower energy, as shown in Figure 9. Once again, a ~300-cm^{-1} progression frequency is seen, and the origin appears at 13 150 cm^{-1}. Both π and σ_2 (not shown) absorption of thick crystals extends to lower energy of the σ_1 (y) absorption, but no structure is apparent.

An x-polarized transition appears at 450 nm. Martin,[1] lacking σ_2 data, suggested that there might be significant z intensity here. Clearly, this is not the case. Instead, we must conclude that the x,y-polarized transition of LRAC at 448 nm (Figure 4) has been strongly split. The y component of the hydrate spectra is evidently at 428 nm (an x,y splitting of 1200 cm^{-1}). The much lower intensity of the y component is also notable.

Two poorly defined absorptions appear at ~380 and ~340 nm. Their intensities both appear to be predominantly z, but significant intensity is certainly present in all polarizations. Finally, the absorption edge to highest energy is x,y polarized.

Assignments

Visible Spectra. We first consider the ~580-nm absorption band. We conclude, in agreement with Martin,[1] that it corresponds to an x,y-allowed transition, hence to a $^1A_{1g} \rightarrow {}^1E_u$ transition of the D_{4h} parent symmetry. However, the previous[1-3] $\pi^*(Rh_2) \rightarrow \sigma^*(Rh_2)$ assignment does not accord with vibronic structure in a ~300-cm^{-1} interval that is now most reasonably attributed to the symmetric Rh–O(carboxylate) stretching frequency of the excited state.

An additional argument against the $\pi^*(Rh_2) \rightarrow \sigma^*(Rh_2)$ assignment comes from the observation of a z-polarized absorption 2000 cm^{-1} below the x,y-polarized transition. Martin et al.[1] noted that the calculations[3] predict $\delta^*(Rh_2)$ (the HOMO) to lie just above π^*, and the observed splitting of the two absorptions is actually in good agreement with the calculated π^*–δ^* splitting. However, the implied assignment of the ~670-nm z-polarized band to $\delta^*(Rh_2) \rightarrow \sigma^*(Rh_2)$ suffers from the drawback that this transition ($b_{1u} \rightarrow a_{2u}$ in D_{4h}) is forbidden even in the $\bar{1}$ site symmetry of the hydrate and also in the $4/m$ site of LRAC.

All of these inconsistencies are removed if we assign the bands of the π^* and δ^* transitions to σ^*(Rh–O(carboxylate)).

The $\pi^*(Rh_2) \rightarrow \sigma^*(Rh-O)$ transition previously[2,3] has been attributed to the ~450-nm absorption and is another $^1A_{1g} \rightarrow {}^1E_u$ x,y-allowed transition in D_{4h} symmetry. The $\delta^*(Rh_2) \rightarrow \sigma^*(Rh-O)$ transition ($b_{1u} \rightarrow b_{1g}$, b_{2u}) is allowed with z polarization in C_{4h} symmetry and in C_{2h} symmetry; the latter is the lowest symmetry including both a rotation (metal–metal) axis and the true $\bar{1}$ site symmetry of the hydrate.[32]

The original assignment[2] of the ~580-nm band to $\pi^*(Rh_2) \rightarrow \sigma^*(Rh_2)$ was based on observations that its position is highly sensitive to axial–ligand variations.[2,27,28] Certainly the $\sigma^*(Rh_2)$ energy is expected[3,33] to be a strong function of such changes, whereas $\sigma^*(Rh-O)$ is not. However, Drago and co-workers[28] have pointed out that π-donor/-acceptor interactions of axial ligands also could affect the $\pi^*(Rh_2)$ orbital energy, and such interactions have been suggested to be important. One unquestionably important effect is that the Rh–Rh bond distance is sensitive to axial ligands,[7,9] and calculations[33,34] show that the π^* energy will vary strongly as a result (since, after all, the metal–metal π–π^* splitting depends on the strength of the metal–metal interaction and hence on the bond length). We thus conclude that our reassignment is not inconsistent with the observed spectral shifts.

The observed vibronic intensity pattern is very reasonable by comparison to established examples of $d\pi \rightarrow d\sigma^*$ transitions of mononuclear complexes.[35,36] Thus, the K_2PtCl_4 emission[35] shows a progression in the symmetric Pt–Cl stretch with a maximum in the (0, 5) transition and a frequency change from 329 cm^{-1} in the ground state to 290 cm^{-1} in the excited state. The similarity to our present observations is consistent with the "ligand field" nature of the assignment.[37,38]

The weak features near 700 nm (Figures 5 and 9) are clearly closely related to the more intense bands just assigned, in view of their similar vibronic structures. Their weakness indicates some sort of forbidden transition, and we suggest that they are the singlet–triplet components of $\pi^*,\delta^*(Rh_2) \rightarrow \sigma^*(Rh-O)$. In the D_{4h} double group these transitions yield two allowed x,y transitions and one allowed z. Both their red shifts from the singlet–singlet transitions and their relative intensities are comparable to those of spin-forbidden $d\pi \rightarrow d\sigma^*$ transitions of mononuclear complexes.[39]

We now turn to the ~450-nm absorption system. Since this absorption maximum is relatively insensitive to axial ligation,[2,27] we cannot simply reverse the literature assignments[2,3] of the visible bands, making this band $\pi^*(Rh_2) \rightarrow \sigma^*(Rh_2)$. Another possible assignment can be obtained from the calculated energy levels. For $Rh(O_2CH)_4(OH_2)_2$, an e_u level is calculated[3a] to be 7000 cm^{-1} (average of component $7b_{2u}$ and $7b_{3u}$ levels) more stable than $\pi^*(Rh_2)$. The composition of this level is predominantly carboxylate ($\sim^2/_3$); following Norman et al.[3] we label it $\pi(Rh-O)$. Because the ~450-nm band is ~5500 cm^{-1} to the blue of $\pi^*(Rh_2) \rightarrow \sigma^*(Rh-O)$, we see that a possible assignment for this x,y-allowed transition is $\pi(Rh-O) \rightarrow \sigma^*(Rh-O)$.

The low metal–metal and axial ligand character of both levels accounts for the insensitivity to axial substitution. More importantly, the predominant carboxylate π character of $\pi(Rh-O)$ provides an explanation for the enormous site effect in the hydrate. Recall that hydrogen bonds are formed with carboxylate oxygens along the y axis but not with those along x. The hydrogen bonding will polarize carboxylate π-electron density away from the rhodium atoms (toward the H bonds) and stabilize levels involving such density. The latter effect is consistent with the ~1200 cm^{-1} higher energy observed for the y component, whereas the former effect may account for the lower intensity of this component. As noted by Martin et al.,[1] the previous assignments[2,3] provided no rationale for a differential splitting of the two $^1A_{1g} \rightarrow {}^1E_u$ transitions.

Finally, we briefly consider the two weak bands near 340 and 380 nm. Since neither seems sensitive to axial ligand substitution, we exclude both axial ligand charge transfer and transitions terminating in $\sigma^*(Rh_2)$ as possible assignments. Our main interest in these bands lies in the prediction from the calculated[3a] energy levels that the $\delta(Rh_2) \rightarrow \sigma^*(Rh-O)$ transition ought to lie near $\pi(Rh-O) \rightarrow \sigma^*(Rh-O)$. The former transforms identically with $\delta^*(Rh_2) \rightarrow \sigma^*(Rh-O)$, so it should be z polarized. Both of the observed weak bands are predominantly z polarized. If either is to be assigned to $\delta(Rh-Rh) \rightarrow \sigma^*(Rh-O)$, we would prefer it to be the ~340-nm band, as the ~380-nm band appears to be vibronically allowed in the LRAC spectra (Figures 3 and 4). But the evidence for this assignment is not compelling.

Ultraviolet Spectra. Because we were not able to extend our single-crystal spectra below λ ~320 nm, our discussion of the UV region will rely primarily upon isotropic spectra. We initially note that axial ligands have a profound effect upon the ultraviolet absorptions.

An extremely intense (ϵ ~25 000) band appears in the near-UV region for the chloride, bromide, and iodide adducts (Figure 2 and Table V). The pronounced red shift as the halide becomes more reducing is similar to that of ligand-to-metal charge-transfer (LMCT) transitions of mononuclear complexes[39,40] and suggests assignment to a transition from a predominantly halide σ-symmetry level to $\sigma^*(Rh_2)$. (The high intensity requires $\sigma \rightarrow \sigma^*$ character.[40]) The necessary $\sigma(M-Cl)$ level turns up just below $\pi^*,\delta^*(M_2)$ in a calculation[3b] on $Ru_2(O_2CH)_4Cl_2^-$, whereas a phosphine σ level is the HOMO for $Rh_2(O_2CH)_4(PH_3)_2$.[33] This transition ($a_{1g} \rightarrow a_{2u}$ in D_{4h}) should be z polarized, consistent with the z polarization of the UV absorption edge seen for LRAC (Figures 3 and 4). The σ-symmetry levels and effects on metal–metal bonding have been extensively discussed.[3,33]

Comparison to mononuclear complexes suggests[40,41] that $\sigma(Rh-NH_3) \rightarrow \sigma^*(Rh_2)$ should be just slightly higher energy than $\sigma(Rh-Cl) \rightarrow \sigma^*(Rh_2)$, and we assign the 265-nm band of $Rh_2(O_2CCH_3)_4(NH_3)_2$ (band III of ref 2) to this transition rather than to $\sigma(Rh_2) \rightarrow \sigma^*(Rh_2)$.[2]

On the other hand, the similarity between the UV spectra of the H_2O and CH_3CN adducts (Table V) suggests that the observed bands are not axial LMCT in these cases, and the calculation for the aquo complex[3a] agrees in predicting the highest energy σ-symmetry level to have mainly Rh_2 character. Relative both to the preceding examples of $\sigma(Rh-X) \rightarrow \sigma^*(Rh_2)$ transitions and to well-established examples of metal–metal $\sigma \rightarrow \sigma^*$ transitions[42] (including Rh(II) isocyanide

(32) Because of the temperature-independent z-polarized intensity of the x,y-polarized transition at ~580 nm, even C_{2h} symmetry is too high for an entirely satisfactory description of this system.
(33) Bursten, B. E.; Cotton, F. A. *Inorg. Chem.* **1981**, *20*, 3042.
(34) Cotton, F. A.; Stanley, G. G. *Inorg. Chem.* **1977**, *16*, 2668.
(35) Yersin, H.; Otto, H.; Zink, J. I.; Gliemann, G. *J. Am. Chem. Soc.* **1980**, *102*, 951.
(36) Wilson, R. B.; Solomon, E. I. *J. Am. Chem. Soc.* **1980**, *102*, 4085.
(37) Franck–Condon calculations[35,36] on the $\pi^*(Rh_2) \rightarrow \sigma^*(Rh-O)$ system of $Rh_2(O_2CCH_3)_4(OH_2)_2$ depend on assumptions about the location of the origin (see Figure 8) as well as the form of the normal mode, especially the "effective mass". In order to fit the profile of the ~580-nm band for any reasonable set of assumptions, 0.1–0.2-Å distortions of individual Rh–O bonds are required.
(38) Obviously, the Franck–Condon factor for $\nu(Rh_2)$ must be fairly small; subprogressions of any great length in this mode would have blurred out the structure in $\nu(Rh-O)$. We think that this is reasonable because $\nu(Rh_2)$ is a low-frequency, hence high-amplitude, mode: if one-electron depopulation of π^* in the excited state were associated with a 0.05-Å decrease in Rh–Rh distance, then the calculated $I_{1,0}/I_{0,0}$ ratio for $\nu(Rh_2)$ = 160 cm^{-1} is only 0.3 (diatomic approximation).
(39) Geoffroy, G. L.; Wrighton, M. S.; Hammond, G. S.; Gray, H. B. *Inorg. Chem.* **1974**, *13*, 430.
(40) Miskowski, V. M.; Gray, H. B. *Inorg. Chem.* **1975**, *14*, 401.
(41) Stein, P.; Miskowski, V.; Woodruff, W. H.; Griffin, J. P.; Werner, K. G.; Gaber, B. P.; Spiro, T. G. *J. Chem. Phys.* **1976**, *64*, 2159.

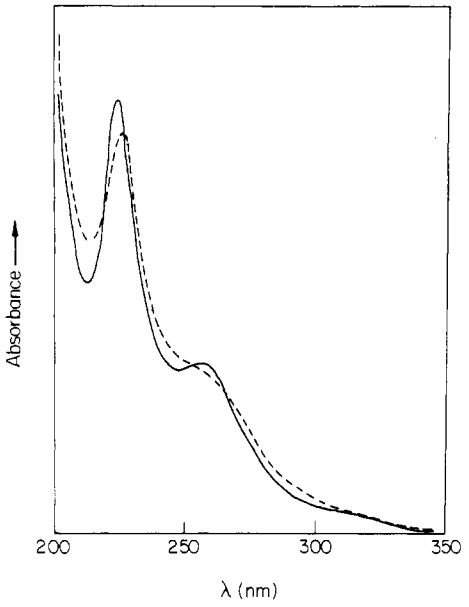

Figure 10. Electronic spectra at 300 (--) and 20 K (—) of $Rh_2(O_2CCH_3)_4(OH_2)_2$ in a PVA film. The spectra are corrected for PVA absorption.

complexes[42d]), we expect $\sigma(Rh_2) \rightarrow \sigma^*(Rh_2)$ to be an intense transition, so assignment to the ~220-nm band of the H_2O and CH_3CN complexes (Table V, Figure 2) is suggested, whereas the 233-nm band of the chloride and the 227-nm band of the NH_3 adduct[2] may represent the same transition shifted somewhat to lower energy by the axial interaction.

Pronounced narrowing and blue-shifting at low temperature are now considered[42] to be positive evidence for a metal–metal $\sigma \rightarrow \sigma^*$ assignment; the low frequency and large Franck–Condon factor of $\nu(M_2)$ are responsible for the thermal behavior. As Figure 10 shows, the 220-nm band of $Rh_2(O_2CCH_3)_4(OH_2)_2$ does show a pronounced thermal effect in a PVA film.

Figure 10 also shows a shoulder resolving near 300 nm at low temperature. This absorption system probably is responsible for the x,y polarization of the single-crystal spectra (Figure 8) at their short-λ limit, and it therefore represents the lowest energy candidate for the still missing $\pi^*(Rh_2) \rightarrow \sigma^*(Rh_2)$ transition. The ~250-nm band, of completely unknown polarization, is also a candidate. Of course, allowed carboxylate-to-rhodium LMCT transitions might also,[3] and probably do, contribute to the UV absorption.

Importantly, we can conclude that the transitions terminating in $\sigma^*(Rh_2)$ appear at wavelengths *no longer* than ~300 nm, thereby allowing us to see an interesting (and satisfying) relationship that was not apparent before this work. The electronic spectra of the isoelectronic compounds with strong-field (usually π-back-bonding) ligands and "long" (2.8–3.0 Å) single metal–metal bonds[7,42] show $\sigma \rightarrow \sigma^*$ transitions in the near-UV to visible region, with $d\pi \rightarrow \sigma^*$ transitions nearby, usually just to lower energy. Thus,[42a] $Mn_2(CO)_{10}$ shows $\sigma \rightarrow \sigma^*$ at 342 nm (ϵ 21 000) and $d\pi \rightarrow \sigma^*$ as a shoulder (ϵ ~3000) at ~390 nm. Comparing to $Rh_2(O_2CCH_3)_4L_2$, we now find that transitions terminating in $\sigma^*(M_2)$ have been strongly shifted into the UV, which we can associate with the much shorter metal–metal bond. Meanwhile, transitions terminating in σ^*(M–equatorial ligand) have been shifted down into the visible, which we can rationalize readily in terms of the much weaker equatorial ligand field.

Comparison to Calculations. For the most part our assignments are in accord with Norman's calculated energy levels.[3] In some cases such as the π(Rh–O) $\rightarrow \sigma^*$(Rh–O) transition, a reasonable assignment would not have been readily apparent without guidance from the calculation. Moreover, the calculated energy for $\pi^*(Rh_2) \rightarrow \sigma^*$(Rh–O) (23 700 cm^{-1})[3b] is as close to the experimental value (17 200 cm^{-1}) as could realistically have been expected when the limitations[43] of the theoretical method that was employed are taken into consideration.

Evidently, the only real failing of the calculation is that it underestimated the energy of $\pi^*(Rh_2) \rightarrow \sigma^*(Rh_2)$ (calculated at 19 700 cm^{-1}). Norman and Kolari[3a] pointed out that the $\sigma(Rh_2) \rightarrow \sigma^*(Rh_2)$ transition energy is expected to be much greater than the ground-state energy level difference (~29 000 cm^{-1}), because of large relaxation effects. (Unfortunately, a spin-polarized transition-state calculation of this excitation energy, which would provide a useful comparison to the other[3b] calculated transition energies, has not been reported.) We suggest that other excitations into $\sigma^*(Rh_2)$ also may be subject to relaxation effects that are not treated adequately by the transition-state calculations.

Rh^{II}–Rh^{II} Bond Strengths. We earlier used a correlation of $\nu(M_2)$ values for carboxylate-bridged complexes to support an assignment[11,12] of $\nu(Rh_2)$ for rhodium acetate. We should now note that a comparison of $\nu(Rh_2)$ for rhodium acetate and the isocyanide-bridged complexes Rh_2(1,3-diisocyanopropane)$_4X_2^{2+}$, which have[42d] similar $\nu(Rh_2)$'s but Rh–Rh distances ~0.4 Å longer, indicates a remarkable failure of Badger's rule,[44] which assumes a regular relationship between bond length and the cube root of the force constant.

The failure is understandable,[45] because the bonds in the two cases involve rather different orbitals. The most thoroughly investigated molecule that possesses a long metal–metal single bond is $Mn_2(CO)_{10}$. A recent calculation[46a] indicates that the σ^* orbital in this molecule is only 41% $3d_{z^2}$; earlier calculations[42a,46b,c] also suggest that 3d orbitals do not account in the main for the bonding, which is attributed to mixing of π^*(carbonyl) and (p_z, s) metal orbitals into the σ/σ^* orbitals.

On the other hand, the $\sigma(Rh_2)$ bond in rhodium acetate is calculated to have primarily $4d_{z^2}$ character (σ^* ~92% d_{z^2}).[3b] We suggest that the different bond lengths in the two cases are simply characteristic of the different orbital components in the bond, presumably modulated by the different ligand bonding modes.

We should finally consider whether the higher $\sigma \rightarrow \sigma^*$ transition energy of rhodium acetate means that it has a stronger metal–metal bond than the "long" M_2-bonded molecules. Unfortunately, a definitive answer cannot be given. Even sidestepping the difficult question of the relationship of one-electron-orbital energy differences and dissociation energies, we cannot even rank the one-electron energy differences experimentally. Since the rhodium acetate bonding orbitals will certainly be less diffuse than those for "long" bonds, two-electron integrals will be larger, and it is recognized[47] that these make important contributions to the energies of bonding–antibonding transitions.

Acknowledgment. We gratefully acknowledge many helpful

(42) (a) Levenson, R. A.; Gray, H. B. *J. Am. Chem. Soc.* **1975**, *97*, 6042. (b) Wrighton, M. S.; Ginley, D. S. *Ibid.* **1975**, *97*, 4246. (c) Abrahamson, H. B.; Frazier, C. C.; Ginley, D. S.; Gray, H. B.; Lilenthal, J.; Tyler, D. R.; Wrighton, M. S. *Inorg. Chem.* **1977**, *16*, 1554. (d) Miskowski, V. M.; Loehr, T. M.; Gray, H. B., to be submitted for publication.

(43) (a) Messmer, R. P.; Salahub, D. R. *J. Chem. Phys.* **1976**, *65*, 779. (b) Aizman, A.; Case, D. A. *J. Am. Chem. Soc.* **1981**, *20*, 528.

(44) Badger, R. M. *Phys. Rev.* **1935**, *48*, 284.

(45) Herschbach, D. R.; Laurie, V. W. *J. Chem. Phys.* **1961**, *35*, 458.

(46) (a) Heijser, W.; Baerends, E. J.; Ros, P. *Symp. Faraday Soc.* **1980**, *No. 14*, 211. (b) Elian, M.; Hoffmann, R. *Inorg. Chem.* **1975**, *14*, 211. (c) Brown, D. A.; Chambers, W. J.; Fitzpatrick, N. J.; Rawlinson, R. M. *J. Chem. Soc. A* **1971**, 720.

(47) Mulliken, R. S. *J. Chem. Phys.* **1939**, *7*, 21.

discussions with Dr. S. F. Rice and Professor D. S. Martin. Several infrared spectroscopic measurements were performed in Professor G. R. Rossman's laboratory at Caltech. This work was supported by National Science Foundation Grant CHE81-20419.

Registry No. $Rh_2(O_2CCH_3)_4(OH_2)_2$, 29998-99-0; $Li_2Rh_2(O_2CCH_3)_4Cl_2 \cdot 8H_2O$, 88945-58-8; $Rh_2(O_2CCH_3)_4Cl_2^{2-}$, 71844-86-5; $Rh_2(O_2CCH_3)_4Br_2^{2-}$, 88945-59-9; $Rh_2(O_2CCH_3)_4I_2^{2-}$, 88968-31-4.

Supplementary Material Available: Listings of Gaussian amplitudes of the non-hydrogen atoms and observed and calculated structure factor amplitudes (8 pages). Ordering information is given on any current masthead page.

Contribution from the Istituto di Teoria e Struttura Elettronica e Comportamento Spettrochimico dei Composti di Coordinazione del CNR, 00016 Monterotondo Stazione, Rome, Italy

Hemiporphyrazine, a Porphyrin-Related Macrocycle That Induces Rhombically Compressed Stereochemistries: Structure and Properties of Bis(pyridine)(hemiporphyrazinato)nickel(II)

E. AGOSTINELLI, D. ATTANASIO,* I. COLLAMATI,* and V. FARES

Received May 24, 1983

The title compound crystallizes in the $P2_1/c$ space group with $Z = 4$, $a = 16.418$ (7) Å, $b = 9.727$ (4) Å, $c = 18.632$ (6) Å, and $\beta = 94.59$ (3)°. The stereochemistry is rhombically compressed with the unique axis defined by the metal isoindole nitrogen atoms, which are 1.97 Å from the nickel ion. The other two Ni–N distances are 2.18 and 2.22 Å, for the macrocyclic and adduct pyridine nitrogen atoms, respectively. In agreement with this, the EPR spectrum of the Cu-doped nickel complex is typical of a predominant $|z^2\rangle$ ground state with a strong rhombic component. Other related complexes were investigated by EPR spectroscopy and found to have a qualitatively similar geometry due to the "elliptical" coordination hole of the hemiporphyrazinato ligand.

Hemiporphrazine, hpH_2 (I), is a highly conjugated, although

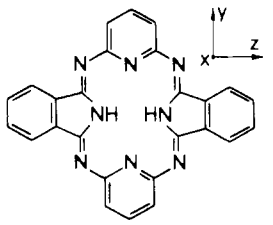

I

nonaromatic (20π), N_4 macrocycle with several structural features in common with porphyrins and phthalocyanines. In spite of this, recent work[1] has shown that the hemiporphyrazinato dianion (hp) exhibits a rather peculiar coordination chemistry partly due to the weakness and asymmetry of its ligand field. Its metal complexes display a marked tendency toward six-coordination. Various adducts with protic donors such as water or hydrohalic acids were investigated and found to be strongly stabilized by proton interaction with the aza groups of the hp ligand.

The EPR spectra of Cu(hp), magnetically diluted in six-coordinated hosts such as $Zn(hp)(HCl)_2$, were typical of a rhombically compressed symmetry, with an essentially $|z^2\rangle$ ground state. This was ascribed to the pronounced ellipticity of the hp coordination hole.[2-4] Apparently, upon axial coordination the unique axis shifts from the normal to the macrocyclic plane to the direction of the strongest metal–ligand bond, i.e. to the metal isoindole nitrogen direction with a simultaneous change of the stereochemistry from rhombically elongated to rhombically compressed.

This behavior, which is induced by the unique geometry of the macrocycle, depends of course on the nature of the central metal ion and on the strength of the axial donors. However, detailed information could not be obtained due to the lack of single crystals suitable for X-ray analysis. For this reason we investigated the interaction of some M(hp) complexes with different N bases and now report the crystal and molecular structure of $Ni(hp)(py)_2$ together with some spectroscopic information concerning this compound and some related Ni(II) and Cu(II) complexes.

Experimental Section

The complexes $Ni(hp)(py)_2$ and $Ni(hp)(4\text{-Mepy})_2$ were obtained by simple crystallization of Ni(hp)[1] from the neat bases. Slow evaporation of a concentrated pyridine solution (100 mg, 4 mL) gave green, prismatic crystals of $Ni(hp)(py)_2$ suitable for X-ray work.

$Ni(hp)(4\text{-Mepy})_2$ is a stable compound, whereas $Ni(hp)(py)_2$ slowly loses the coordinated base converting to the dihydrate derivative in a few weeks. Anal. Calcd for $C_{36}H_{24}N_{10}Ni$ (py derivative): C, 65.98; H, 3.69; N, 21.37. Found: C, 66.3; H, 3.84; N, 21.6. Calcd for $C_{38}H_{28}N_{10}Ni$ (4-Mepy derivative): C, 66.78; H, 4.13; N, 20.50. Found: C, 66.6; H, 4.2; N, 20.3.

Preparation of the Cu(II) and Zn(II) analogues was attempted in a similar way, but the starting materials Cu(hp) and $Zn(hp)H_2O$ were recovered unchanged after crystallization. The Cu-doped Ni(II) complexes were prepared by cocrystallization using ca. 2% of $^{63}Cu(hp)$ (^{63}Cu obtained from Oak Ridge National Laboratories in the form of ^{63}CuO). The EPR spectra were measured on freshly crystallized samples. After 1 or 2 days, $Cu/Ni(hp)(py)_2$ gives a drastically different spectrum, presumably due to loss of the coordinated base.

Elemental analyses and physical measurements were performed as previously reported.[1]

Crystal Data. $C_{36}H_{24}N_{10}Ni$: mol wt. 655.368, monoclinic, $a = 16.418$ (7) Å, $b = 9.727$ (4) Å, $c = 18.632$ (6) Å, $\beta = 94.59$ (3)°, $V = 2966$ (2) Å^3, $\rho_{obsd} = 1.47$ (2) g·cm^{-3} (by flotation), $Z = 4$, $\rho_{calcd} = 1.468$ g·cm^{-3}, $F(000) = 338$, space group $P2_1/c$ (No. 14), systematic presences $h0l$ ($l = 2n$), $0k0$ ($k = 2n$), Mo Kα radiation $\lambda = 0.71069$ Å, μ(Mo Kα) = 7.19 cm^{-1}.

Structure Solution and Refinement. Diffraction data were collected from a crystal of approximate dimensions 0.1 × 0.1 × 0.5 mm on a Syntex $P2_1$ diffractometer with graphite-monochromated Mo Kα radiation by the θ–2θ scan technique ($2\theta_{max} \leq 50$).

Intensity data were corrected for Lorentz and polarization effects. Given the low value of μ and the crystal dimensions, no absorption correction was applied. A set of 1726 independent reflections ($I > 3\sigma(I)$) was used for solution by standard heavy-atom techniques. The structure was refined by a full-matrix least-squares method based on minimization of the function $w(|F_o| - |F_c|)^2$ where $w = 1/\sigma^2(F_o)$ and

(1) Attanasio, D.; Collamati, I.; Cervone, E. *Inorg. Chem.* **1983**, *22*, 3281.
(2) Speakman, J. C. *Acta Crystallogr.* **1953**, *6*, 784.
(3) Bissell, E. C. Ph.D. Thesis, Case Western University, 1970, University Microfilms No. 70-25, p 849.
(4) Hecht, H. J.; Luger, P. *Acta Crystallogr., Sect. B* **1974**, *B30*, 2843.

0020-1669/84/1323-1162$01.50/0